Imaging the Distribution of Magnetic Nanoparticles on Animal Bodies Using Scanning SQUID Biosusceptometry Attached With a Video Camera

J. J. Chieh, H. E. Horng, W. K. Tseng, S. Y. Yang, C. Y. Hong, H. C. Yang, and C. C. Wu

***Abstract*—To image magnetic nanoparticles (MNPs) on animal bodies, physicians often use magnetic resonance imaging to determine the superparamagnetic characteristics of MNPs during preoperative analysis. However, magnetic resonance imaging is unsuitable for other biomedical applications, such as the curative surgical resection of tumors or pharmacokinetic studies of MNPs, because of the requirement of nonmetal environments and high financial cost of frequent examination, respectively. Thus, researchers have proposed other nonmagnetic imaging technologies, such as fluorescence, using multimodal MNPs with nonmagnetic indicators. The development of a magnetic instrument based on the other magnetic characteristics of MNPs avoids the disadvantages of multimodal MNPs, including the biosafety risk. On the basis of the alternating current susceptibility of MNPs, previous research has demonstrated the magnetic examination of scanning superconducting-quantum-interference-device biosusceptometry (SSB). This study, using a low-noise charge-coupled-device type of a video camera, reports the integration of SSB and charge-coupled-device to immediately image the magnetic signals on animal bodies or organic tissue. This real-time imaging by SSB increases the usefulness of MNPs for more clinical applications, including the imaging-guided curative surgical resection of tumors.**

***Index Terms*—AC susceptibility, magnetic nanoparticles, scanning SQUID biosusceptometry, video camera.**

I. Introduction

MAGNETIC nanoparticles have been widely applied in biomedical fields for immunoassays [1], controlling hyperthermia [2], [3], nanosurgery [4], drug delivery [5], [6], and image contrast of MRI [7], [8]. Because of their low toxicity risks, MNPs are far superior to other materials, such as those that are fluorescent, exhibit radioactivity, and other magnetic materials of gadolinium, for animal testing. However, each instrument has intrinsic operation limitations in each MNP application. For example, MRI has the serious requirement of a shielding environment and complex analysis, and is therefore limited to preoperative diagnosis. For real-time guiding of curative surgical resection of tumors targeted by antibody-mediated MNPs, metal surgical tools limit the use of MRI.

To compensate for the difficulties of using MNPs in these applications, researchers have developed multimodal MNPs with fluorescent or radioactive properties for other nonmagnetic methods [9], [10]. These complex MNPs not only increase toxicity risks, but also the cost. Even for the example of the imaging-guided curative surgical resection of tumors using fluorescence [11], the short lifespan of fluorescence makes clinical surgery difficult.

Thus, the superior magnetic characteristics of MNPs should be studied to develop more magnetic instruments beyond MRI. Previous studies presented an SSB approach using AC susceptibility for the in vivo examination of MNPs in animals [12], [13]. However, the functions of SSB should be upgraded from using only magnetic properties to enable imaging-guided applications. This is because optical images allow physicians to see exactly where MNPs are distributed. The system proposed in this study attaches a low-noise CCD-type video camera to the scanning-coil unit of the SSB system. This integration of SSB and CCD can immediately image the magnetic signals on animal bodies or organic tissue. The real-time mapping of magnetic images to the CCD image is applicable to many biomedical applications, including the metabolism study of MNPs and the imaging-guided curative surgical resection of tumors.

II. System Description

The scanning SQUID biosusceptometry system in this study consisted of a SQUID unit and a scanning-coil unit (Fig. 1(a)) [12], [13]. In the SQUID unit, the high-T_c RF SQUID sensor was cooled in the Dewar and shielded in the shielding can. The input coil surrounding SQUID sensors was connected to the input coil by a shielded and twisted copper wire. The design of the turn numbers and coil sizes for the input coil and pickup coil was optimized based on the transferring theory [14]. The scanning-coil unit consisted of double-shaped pickup coils and

Manuscript received October 8, 2012; accepted November 15, 2012. Date of publication November 21, 2012; date of current version January 25, 2013. This study was supported in part by the National Science Council of Taiwan under Grant NSC100-2221-E003-013, Grant NSC100-2112-M003-010, Grant NSC 100-2120-M-002-015, Grant NSC101-2120-M168-001, and Grant NSC 101-2221-E003-005; and by the Department of Health under Grant DOH99-TD-N-111-008, Grant DOH100-TD-N-111-008, and Grant DOH101-TD-N-111-004.

J. J. Chieh, H. E. Horng, and S. Y. Yang are with the Institute of Electro-Optical Science and Technology, National Taiwan Normal University, Taipei 116, Taiwan (e-mail: phyfv001@scc.ntnu.edu.tw).

W. K. Tseng is with the Institute of Electro-Optical Science and Technology, National Taiwan Normal University, Taipei 116, Taiwan, and also with E-Da Hospital, Kaohsiung 82445, Taiwan.

C. Y. Hong is with the Graduate Institute of Biomedical Engineering, National Chung Hsing University, Taichung 402, Taiwan.

H. C. Yang is with the Department of Electro-Optical Engineering, Kun Shan University, Tainan 710, Taiwan.

C. C. Wu is with the Departments of Internal Medicine and Primary Care Medicine, College of Medicine, National Taiwan University, Taipei 100, Taiwan (e-mail: chauchungwu@ntu.edu.tw).

Color versions of one or more of the figures in this paper are available online at http://ieeexplore.ieee.org.

Digital Object Identifier 10.1109/TASC.2012.2229778

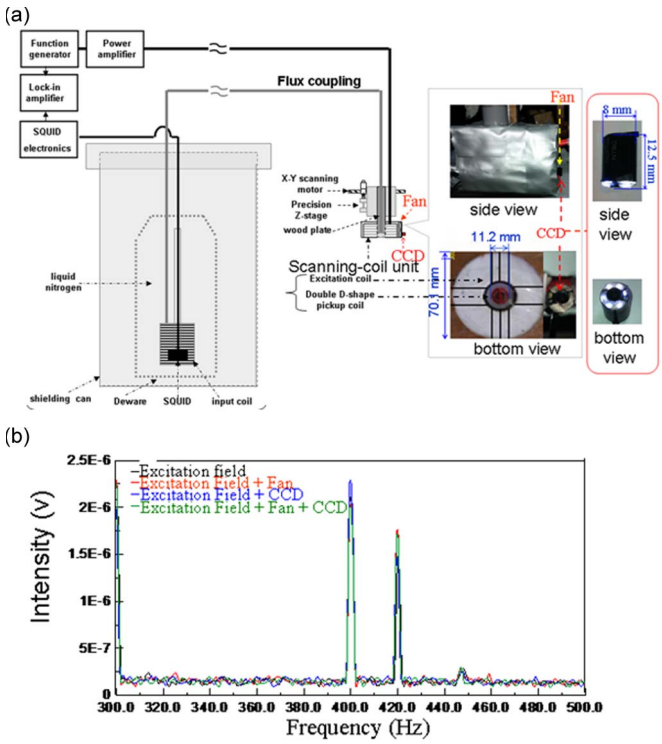

Fig. 1. Specifics of scanning SQUID biosusceptometry and an attached CCD. (a) Scheme and (b) the noise spectrum after the attachment of the used fan and CCD to the scanning-coil unit.

a cylindrical excitation coil. The double-shaped pickup coil is one of first-order pickup coil for scanning along contours. The excitation field at the circle of the excitation coil was 120 Oe in strength and 400 Hz in frequency, and the product of frequency and strength was much lower than the electromagnetic biosafety limit of 4.85×10^8 kA/m · s [15]. To effectively cool the excitation coil, a plastic cage surrounding the excitation and a fan served as a cooling mechanism. To map the magnetic signals on the scanned torso, a color CCD measuring 8 mm in diameter with LED illumination was attached to the fan and aligned with the pickup coil in a line parallel to the scanning path. The entire scanning-coil unit was moved by a three-axial stepping motor controlled by a computer software.

Although the pickup coil was designed to suppress the environmental noise, the close attachment of the fan and CCD made it difficult to avoid noise. Because some harmonics of the fan motor drive frequency at 360 and 420 Hz was found, the measurement frequency of 400 Hz was set between fan harmonics. Fig. 1(b) shows that there was no significant difference in the noise spectrum between only excitation field and all devices of an excitation coil, the used CCD and fan. This proves that the pickup coil suppressed the noise from not only the attached electrical devices, but also the environment.

III. Experiments and Discussion

A. Phantom Test

To evaluate the imaging ability of the proposed system, a hole with a half-ball shape of 2.1 cm in diameter was filled with magnetic fluid (MF) in an ice-making box. The concentration of MF, consisting of water, MNPs of Fe_3O_4, and dextran coating in the hydrodynamic diameter of 57.3 nm, was 0.3 emu/g. The distance between the scanning-coil unit and the plate of the ice-making box was 2 mm. The scanning speed was 0.5 cm/s for each scanning path of 9 cm, and the interval of each scanning path was 0.5 cm.

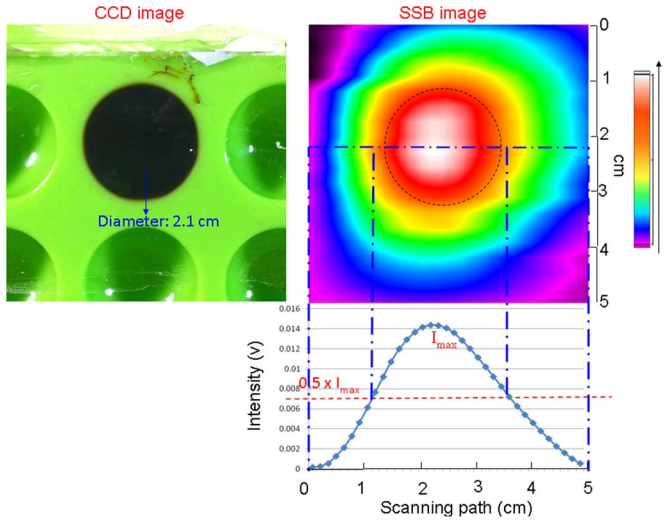

Fig. 2. CCD image and SSB image of a phantom.

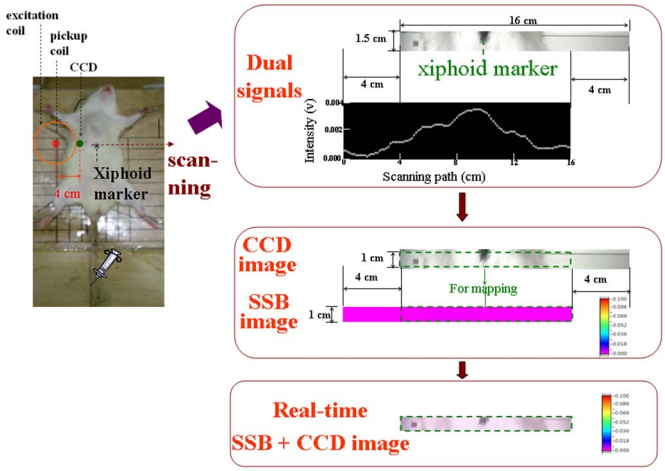

Fig. 3. Mapping process of SSB image and CCD image.

After the scanning process, both the CCD image and SSB image were cut to a common length of 5 cm (Fig. 2). To evaluate the MF distribution, half of the maximum intensity, equal to the dark orange color in the SSB image, was used as the criterion. The dark orange contour shows a similar circular shape. The dark orange area is approximately 0.2 cm larger than the black dotted circle, representing the real MF distribution. This means that this criterion is reliable for the analysis of MNP distribution in SSB images.

B. In Vivo Test

A Wistar rat 5 weeks old was anesthetized and aligned on a wooden plate with coordinate lines of 2 cm. A 0.9 mL volume of MF at a 0.3 emu/g concentration was injected into the tail veins of the anesthetized rat. Fig. 3 shows the dual signals from SSB and CCD.

For example, the rat xiphoid was marked as the significant black markers. After the scanning-coil unit scanned across the xiphoid, dual signals of CCD and the magnetic signals were obtained with the shift of 4 cm, the interval between the center of pickup coil and that of excitation coil. Consequently, a

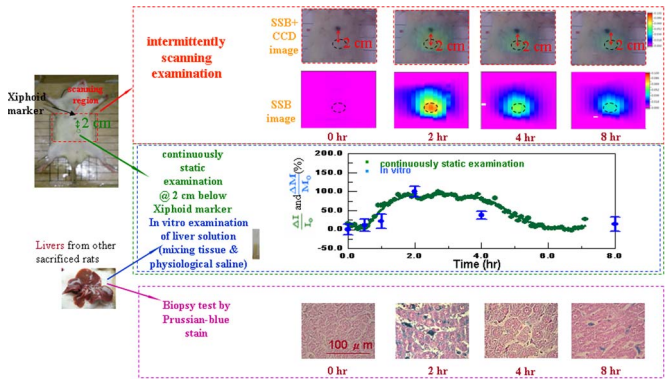

Fig. 4. Comparison between intermittently scanning examination, continuously static examination [12], and biopsy test [13].

2-dimensional SSB image with 1 cm in width was constructed from the magnetic signal because the diameter of the pickup coil was approximately 1 cm. The CCD image was also cut to the same size as the SSB image. All image processing was performed automatically by a computer program.

This intermittent scanning process was performed at 0 h (before the injection of MF), 2 h, 4 h, and 8 h after the injection of MF. Fig. 4 shows the mapping images from SSB images and CCD images. This figure indicates that the intensity and distribution of magnetic signals was almost none at 0 h, reached the highest and widest level at 2 h, decreased at 4 h, and was the weakest at 8 h. These results indicate that the MNP distribution in the liver (below the xiphoid and within the abdomen) was zero before the MF injection, reached the highest concentration and most extensive spread at 2 h after MF injection, and decreased with time from 4 to 8 h after the MF injection. Based on the criterion of 0.5 $I_{\max}$ as the major MNP distribution, a black dotted line was marked on both SSB image and SSB+CCD image. The SSB+CCD image showed that the major MNP distribution was 2 cm below and apart from the xiphoid. This finding confirms the biological position of livers. From the SSB image, the magnetic signal at the center of major MNP distribution reached the maximum level at 2 h, and decreased with time. This variation with time was the same as the results of continuously static examination at 2 cm below the xiphoid marker [13]. This also agrees with not only the results of in vitro examination, but also a biopsy test [12], [13]. The samples of the last two examinations were taken from the liver. The former sample was a mix of liver tissue and physiological saline, and the latter was only liver tissue stained with Prussian blue. Therefore, more MNPs in liver tissue expressed higher magnetic intensity, and more blue spots caused by iron from the Fe_3O_4 composition of MNPs. Based on the good agreement among the results of the intermittent scanning examination, continuous static examination, and biopsy testing, intermittent scanning examination by SSB can be used as a future clinical methodology. The continuously static examination by SSB is unsuitable for the long-term examination of animals, and the biopsy test involves significant risks, despite being the current gold standard.

The results of this study show that SSB operation has the characteristics of lower consumption of excitation power, low risk of biosafety concerns, easy scanning of a large area of the animal torso, an unshielded environment, and enough spatial resolution (several millimeters) for most clinical applications. However, this current scheme of SSB is against 3D positioning of MNPs. MRI and magnetic particle imaging (MPI) [16] work because these technologies have excitation mechanisms with not only high static or gradient fields of several Tesla, but also a high frequency of AC fields. These characteristics create the need for a shielded environment for safety considerations, have a limited field-of-view region, and risk tissue damage from MNP heating or RF heating. Because of the clinical merit of distributing MNPs only in related biological positions, it is necessary to map MPI images to MRI images as SSB+CCD image in this work.

IV. Conclusion

This study confirms the feasibility of imaging the distribution of MNPs on animal bodies using an SSB+CCD system. The proposed method is reliable for the study of MNP metabolism through good agreement between intermittently scanning examination, continuously static examination, and biopsy tests. This approach can be used for imaging-guided curative surgical resection of tumors targeted with antibody-coated MNPs.

References

[1] C. Y. Hong, C. C. Wu, Y. C. Chiu, S. Y. Yang, H. E. Horng, and H. C. Yang, "Magnetic susceptibility reduction method for magnetically labeled immunoassay," *Appl. Phys. Lett.*, vol. 88, p. 212512, 2006.

[2] R. E. Rosensweig, "Heating magnetic fluid with alternating magnetic field," *J. Magn. Magn. Mater.*, vol. 252, pp. 370–374, 2002.

[3] H. Y. Tseng, G. B. Lee, C. Y. Lee, Y. H. Shin, and X. Z. Lin, "Localised heating of tumours utilizing injectable magnetic nanoparticles for hyperthermia cancer therapy," *IET Nanobiotechnol.*, vol. 3, pp. 46–54, 2009.

[4] B. G. Nair, Y. Nagaoka, H. Morimoto, Y. Yoshida, T. Maekawa, and D. S. Kumar, "Aptamer conjugated magnetic nanoparticles as nanosurgeons," *Nanotechnology*, vol. 21, p. 455102, 2010.

[5] E. Duguet, S. Vasseur, S. Mornet, and J. M. Devoisselle, "Magnetic nanoparticles and their applications in medicine," *Nanomedicine*, vol. l, pp. 157–168, 2006.

[6] S. Prijic and G. Sersa, "Magnetic nanoparticles as targeted delivery systems in oncology," *Radiol. Oncol.*, vol. 45, pp. 1–16, 2011.

[7] S. H. Liao, H. C. Yang, H. E. Horng, and S. Y. Yang, "Characterization of magnetic nanoparticles as contrast agents in magnetic resonance imaging using high-Tc superconducting quantum interference devices in microtesla magnetic fields," *Supercond. Sci. Technol.*, vol. 22, p. 025003, 2009.

[8] J. Qiao, S. Li, L. Wei, J. Jiang, R. Long, H. Mao, L. Wei, L. Wang, H. Yang, H. E. Grossniklaus, Z. R. Liu, and J. J. Yang, "HER2 targeted molecular MR imaging using a de novo designed protein contrast agent," *PLoS ONE*, vol. 6, p. e18103, 2011.

[9] M. F. Kircher, U. Mahmood, R. S. King, R. Weissleder, and L. Josephson, "A multimodal nanoparticle for preoperative magnetic delineation resonance imaging and intraoperative optical brain tumor," *Cancer Res.*, vol. 63, pp. 8122–8125, 2003.

[10] K. L. Watkin and M. A. McDonald, "Multi-modal contrast agents: A first step," *Academ. Radiol.*, vol. 9, pp. S285–S289, 2002.

[11] X. Ni, J. Yang, and M. Li, "Imaging-guided curative surgical resection of pancreatic cancer in a xenograft mouse model," *Cancer Lett.*, vol. 324, pp. 179–185, 2012.

[12] J. J. Chieh, W. K. Tseng, H. E. Horng, C. Y. Hong, H. C. Yang, and C. C. Wu, "In-vivo and real-time measurement of magnetic-nanoparticles distribution in animals by scanning SQUID biosusceptometry for biomedicine study," *IEEE Trans. Biomed. Eng.*, vol. 58, pp. 2719–2724, 2011.

[13] J. J. Chieh and C. Y. Hong, "Non-invasive and high-sensitivity scanning detection of magnetic nanoparticles in animals using high-T_c scanning superconducting-quantum-interference-device biosusceptometry," *Rev. Sci. Instrum.*, vol. 82, p. 084301, 2011.

[14] T. Kondo and H. Itozaki, "Normal conducting transfer coil for SQUID NDE," *Supercond. Sci. Technol.*, vol. 17, pp. 459–462, 2004.

[15] D. A. Hill, "Further studies of human whole-body radiofrequency absorption rates," *Bioelectromagnetics*, vol. 6, pp. 33–40, 1985.

[16] B. Gleich and J. Weizenecker, "Tomographic imaging using the nonlinear response of magnetic particles," *Nature*, vol. 435, pp. 1214–1217, 2005.